Discrete Modeling of the Mechanics of Entangled Materials

David Rodney, Marc Fivel, and Rémy Dendievel

Génie Physique et Mécanique des Matériaux (UMR CNRS 5010), Institut National Polytechnique de Grenoble, ENSPG, 101 rue de la Physique, Saint Martin d'Hères Cedex BP 46 38402, France

(Received 31 March 2005; published 2 September 2005)

We employ a discrete computational model to study the entanglement transition of non-cross-linked semiflexible fibers during isostatic compressions. We determine, as a function of the fiber aspect ratio, packing densities and caging numbers, i.e., the density and number of contacts per fiber at the entanglement transition. The caging number is found to be 8 for short fibers and to drop down to 4 for longer fibers. Compressions beyond the entanglement transition allow us to determine, for these networks that deform primarily by bending, the scaling exponents of the pressure and of the bulk modulus (= 3), as well as of the number of contacts per fiber (= 1).

DOI: 10.1103/PhysRevLett.95.108004 PACS numbers: 81.05.Lg, 62.20.Dc, 87.16.Ac

Fibrous entangled materials are at the heart of several fields of material science. One area of very active research concerns *biopolymers,* with special attention paid to the cytoskeleton, a network of cross-linked protein filaments (F-actin) responsible for the mechanical properties of eucaryotic cells [1]. A second example is the technologically attractive *carbon nanotube-reinforced polymers* [2], where one tries to take advantage in the composite of the high mechanical and electrical properties of the nanotubes. *Papers and fabrics* are other examples of fibrous materials [3,4], which are inherently three dimensional, although one dimension is much smaller than the two others. All these examples have in common that the fibers are *semiflexible;* i.e., their bending stiffness is neither negligible (flexible-coil limit) nor infinite (rigid-rod limit).

Although the behavior of individual semiflexible fibers is now well established [5,6], the mechanics of an assembly of such fibers remains unclear. The systems are known to undergo a mechanical transition, called the *entanglement transition,* when the fiber volume fraction increases. This transition has been studied by oscillating straining experiments on solutions (i.e., no permanent cross-links) of F-actin [7–11]. The frequency-independent plateau modulus G_0 was found to increase rapidly, as c^γ, where c is the polymer concentration, with a scaling exponent $\gamma = 2 \pm 0.3$. On the other hand, Schofield [12] and van Wyk [13] (see Ref. [14] for a recent review) found a different exponent, equal to 3, for the pressure and the Young's modulus of wads of wool compressed uniaxially. van Wyk [13] rationalized this exponent by analyzing the mechanics of 3D fiber networks through the statistics of contact formation and the scaling laws of bending beams.

The entanglement transition was studied by numerical simulations in three dimensions only in the case of rigid rods [15]: random sets of rods of varying aspect ratios were compressed isostatically up to their *packing density,* i.e., the lowest density at which mechanical equilibrium is achieved under a nonzero applied pressure, and the *caging number,* which is the average number of contacts a given fiber experiences, was computed at the transition. In agreement both with experiments and with the *random contact model* [14,16], which essentially assumes straight soft-core fibers positioned and oriented at random, the packing density ρ_c was found to decrease with increasing fiber aspect ratios $\alpha = L/D$, as $\rho_c = 5.1/\alpha$. However, the fibers being rigid, the networks could not be compressed beyond their packing density. To our knowledge, deformation beyond the packing density has been simulated in only two dimensions, in the case of random networks of semiflexible cross-linked fibers [17–19].

In this Letter, we employ a 3D discrete model of semiflexible fibers in interaction, which allows one to compress fiber networks beyond their packing density. We focus on relatively stiff fibers with no permanent cross-links and study the entanglement transition as a function of the fiber aspect ratio. We evaluate from the simulations packing densities and caging numbers at the transition and also compress the networks beyond the transition and extract the scaling exponents of the energy, as well as of the pressure and of the bulk modulus.

Semiflexible fibers are modeled using molecular dynamics techniques developed for the simulation of polymers [20]. The fibers are discretized by nodes whose positions are the degrees of freedom of the model. Traction and bending stiffnesses, as well as nonpenetrability between fibers are modeled by means of a potential energy, given in Eq. (1), where D is the fiber diameter.

$$E = \sum_{(i,i+1)\text{consecutive}} \frac{K_S}{2}\left(1 - \frac{r_{i,i+1}}{D}\right)^2 + \sum_{(i-1,i,i+1)\text{consecutive}} \frac{K_B}{2}(\theta_i - \pi)^2 + \sum_{(i,j)\text{nonconsecutive}} \frac{K_I}{2} H(D - r_{i,j})\left(1 - \frac{r_{i,j}}{D}\right)^{5/2}. \quad (1)$$

The traction stiffness of the fibers is modeled by linear springs between consecutive nodes [first sum in Eq. (1)],

with the fiber Young's modulus controlled by K_S. A bending stiffness is introduced by means of angular springs between consecutive pairs of nodes [second sum in Eq. (1)]. The fibers considered here are straight under no stress, with an equilibrium angle $\theta = \pi$. It can be shown analytically that, in a bending test where a fiber is clamped at one end and subjected to a force F perpendicular to its other end, the usual elasticity law is recovered [21] in the limit of small deformation, with a deflection $\delta = FL^3/3\kappa$ and an effective bending modulus $\kappa = K_B.D/(1 - D/L)(1 - D/2L)$, which weakly depends on the fiber aspect ratio. Interaction between fibers is modeled by a repulsive pair potential [third sum in Eq. (1), with $H(x)$ the Heaviside step function], which acts when the distance between nonconsecutive nodes becomes less than the fiber diameter D, i.e., when the fibers indent each other. The repulsive potential was chosen as Hertz contact potential for elastic indentation between spheres [22]. The fibers are therefore viewed as necklaces of beads of diameter D whose number is equal to the fiber aspect ratio $\alpha = L/D$. The volume of the fibers is computed from the equivalent capped cylinder with the relative density given by $\rho = \pi D^3(3\alpha - 1)/12 \times N_F/V$, where N_F is the number of fibers and V the volume of the cell. The potential energy used here is the 3D-discretized version of the Hamiltonian used in 2D [17–19], augmented by a repulsive potential to treat the nonpenetrability between fibers.

We performed *isostatic compressions* (isodeformation in all three directions) of assemblies with aspect ratios ranging from 10 to 100. The fibers are initially placed and oriented at random [23] in a cubic cell with periodic boundary conditions. Finite size effects become negligible when the cell size is greater than 1.5 times the fiber length, leading to $N_F = 400$ fibers for aspect ratios up to 50 and 750 fibers for an aspect ratio of 100. The set of nondimensional parameters mainly used here is $K_S/K_B = 1.0$, $K_I/K_B = 1.0$, which corresponds to relatively stiff fibers.

The cell size is decreased incrementally, with the fibers translated affinely at the beginning of each increment. Static relaxations are performed during the increments, in order to obtain equilibrium configurations. The most efficient energy minimization algorithm for these very low density systems consists in applying the VERLET algorithm [20], with the nodal inertial term set to zero whenever the product of the force on a node times its velocity is negative. The nondimensional integration parameter used was $K_B\delta t^2/mD^2 = 0.16$. The number of relaxation steps per increment was set to 2×10^6, a choice that is discussed below.

One difficulty in the simulations is that, since the repulsive force between nodes goes to zero when the indentation decreases, the rate of separation also vanishes, and there are many contacts with very small indentations. We checked that by computing the number of contacts as pairs of nonconsecutive nodes closer than an *effective diameter* $0.996D$, the number of contacts is independent of the choice of the effective diameter. Care was also taken not to count redundant contacts when several nodes take part in one contact.

We use the present computational model to study the entanglement transition of networks as a function of the fiber aspect ratio. Figures 1(a) and 1(b) show, respectively, the number of contacts per fiber (i.e., the average number of contacts each fiber experiences) and the energy per fiber, taken at the end of each compression increment, as a function of the relative density. Simulations for two different initial random configurations are shown.

Entanglement transitions are clearly visible in these figures. In the course of the compressions, the systems evolve from a *free-fiber state* at low densities, where the fibers do not interact at equilibrium and both the number of contacts and the energy are zero, to an *entangled state* where the fibers strongly interact and lock each other, with a finite number of contacts and an energy that increases rapidly with the density (similar behaviors are obtained for the pressure and the bulk modulus). Between these two states, there is a *transition region* reminiscent of second-order phase transitions: the number of contacts decreases very slowly during the relaxations and the systems are not equilibrated at the end of the increments, even after 2×10^6 relaxation steps. Data in these regions are shown with smaller open symbols; they are only indicative, since the systems are not relaxed and longer simulations would yield smaller contact numbers and energies. The end of the transition region corresponds to the first increment for which the number of contacts stabilizes within the increment. The first data points outside the transition regions are shown with filled (red online) symbols.

In order to limit the extent of the transition region, one has either to consider larger assemblies or to perform more relaxation steps per increment. Both solutions are computationally expensive. Four hundred fibers and 2×10^6 relaxation steps per increment appeared to be a good compromise with limited transition regions and negligible size effects outside these regions. Indeed, in Fig. 1, the compressions of the two random configurations coincide in the entangled state. Moreover, we checked by using different cell sizes that the relaxed data in the entangled state are independent of the cell size.

In random networks of noninteracting fibers, the number of contacts per fiber increases linearly with the density. By way of contrast, in the present case where the fibers repel each other and are allowed to relax, the number of contacts jumps from zero to a finite value across the transition region. Simultaneously, as shown in Fig. 1, the energy, and also the pressure and the Bulk modulus, starts to deviate from zero. The density at the end of the transition region is therefore the *packing density.* Also, the number of

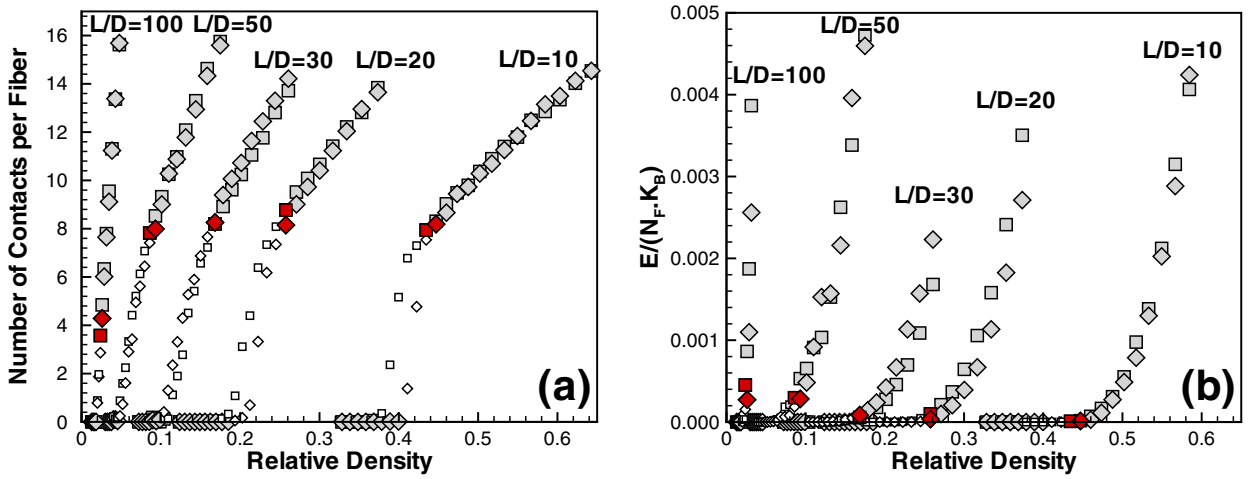

FIG. 1 (color online). (a) Number of contacts per fiber and (b) energy per fiber as a function of relative density, for various aspect ratios (noted in the figure). Compressions of two initially different random networks are shown (squares and diamonds). Nonrelaxed data in the transition regions are indicated with smaller open symbols (see text).

contacts is the *caging number.* Figure 1 reveals that this number is almost constant for short fibers with aspect ratios less than 50 and is close to 8. It drops down to 4 for longer fibers with an aspect ratio of 100. Williams and Philipse [15], using the *mechanical contraction method* for rigid rods, found caging numbers between 6 and 8 for short rods that decrease to 3 for longer rods with aspect ratios above 100. The present caging numbers are larger because of the flexibility of the fibers: the fibers can bend between contacts and more contacts are necessary to lock the fibers. This effect will become more pronounced when considering more flexible fibers, as emphasized at the end of this Letter.

Figure 2 reports the packing density as a function of the fiber aspect ratio and shows that these data agree with the experiments and simulations of Williams and Philipse [15] for rigid rods. The packing density can be fitted by an inverse law $\rho_c = 4.6/\alpha$, although there are deviations, in particular, for large aspect ratios. This is a consequence of the flexibility of the lines which, being bent, can, at a given density, come into contact with more fibers than straight rods, thus lowering the packing densities. Note that in the *random contact model,* the factor relating packing density and aspect ratio is equal to half the caging number. Indeed, $2 \times 4.6 = 9.2$ is close to 8, as found in Fig. 1.

We now turn our attention to the behavior of the networks beyond their packing density. Figure 3 is a compilation of the energy per fiber beyond the packing densities, for aspect ratios greater than 10. This log-scale plot shows that the energy follows a scaling law $E/N_F \sim (\rho - \rho_c)^\alpha$

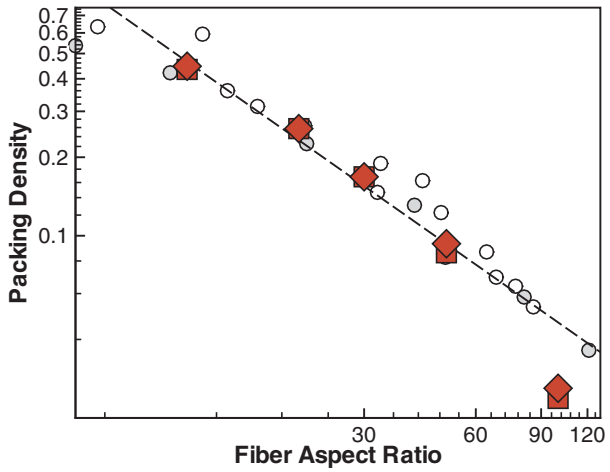

FIG. 2 (color online). Packing density as a function of fiber aspect ratio. Present data (squares and diamonds) are compared to experimental (open circles) and simulated (filled circles) obtained on rigid rods [15]. The dashed line is $\rho_c = 4.6/\alpha$.

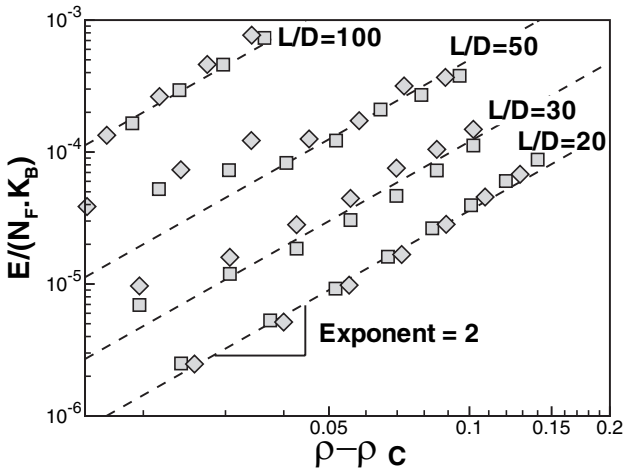

FIG. 3. Log-scale plot of the energy per fiber as a function of the difference between network density and packing density, for various aspect ratios noted on the figure. The curves were shifted with respect to each other for the sake of clarity.

with a single scaling exponent independent of the fiber aspect ratio, $\alpha = 2$. The pressure is derived from the energy, $P = -dE/dV \sim \rho^2(\rho - \rho_c)^{\alpha-1}$, and the bulk modulus is $B = Vd^2E/dV^2 \sim \rho^2(\rho - \rho_c)^{\alpha-2} \times \{(\alpha + 1)\rho - 2\rho_c\}$. These relations have been checked directly from the simulations, using the nodal expressions of the pressure ($P = \mathbf{F} \cdot \mathbf{r}/3V$, where $\mathbf{F}$ and $\mathbf{r}$ are the global force and position vectors, respectively). In the limit of long fibers with large aspect ratios, the packing density ρ_c vanishes and both the pressure and the bulk modulus scale as ρ^β, with a scaling exponent $\beta = \alpha + 1 = 3$. This exponent agrees with that found from dimensional analysis by van Wyk [13] in the case of compressed 3D networks of fibers which deform by bending. It is larger than the one obtained experimentally for the plateau modulus of solutions of biopolymers, which is close to 2 [7–11]. Note, however, that the plateau modulus is related to the shear modulus, and it is well known, for example, in the case of cellular materials [24], that different elastic moduli may have different scaling exponents depending on the material microstructure.

The present networks deform primarily by *bending,* since the uniaxial deformation of the fibers never exceeds 0.05% and corresponds to the stretching necessary to equilibrate the bending forces at the nodes. Moreover, the bending energy is about 10 times larger than both the stretching and the interaction energies. Also, Fig. 1(a) shows that the number of contacts per fiber increases linearly beyond the transition, in agreement with the random contact model. The networks should therefore be viewed as random isotropic networks of fibers that bend between their contact points in order to avoid each other. The present systems are different from cross-linked polymers or open-cell foams since, in the case of an isostatic compression, these materials deform by the uniaxial compression of the fibers, with a bulk modulus linearly proportional to the density [24,25]. The present networks behave differently because, in the absence of permanent cross-links, the fibers can slide with respect to each other, which suppresses all compressions along the fibers. Note that short fibers with an aspect ratio of 10 are too short to bend; they strongly indent each other and do not follow the same scaling law.

Finally, we studied the influence of the flexibility of the fibers by performing simulations with smaller bending coefficients: $K_S/K_B = K_I/K_B = 10$ and $K_S/K_B = K_I/K_B = 100$. In summary, we find that the entanglement transition becomes more gradual with larger caging numbers. This effect is more pronounced for larger aspect ratios. This trend could be expected because, as the fibers are more flexible, they can bend more between contacts and more contacts are needed to lock the fibers.

The present work opens the way to several studies, in particular, the influence of the polydispersity as well as the degree of cross-linking, which can be introduced straightforwardly in the present computational model by placing springs between a given fraction of contacts. The mode of deformation should evolve from bending to uniaxial compression of the fibers as the density of cross-links increases.

The authors thank Ferenc Jarai-Szàbò who greatly participated in the development of the code. We also thank Professor Yves Bréchet for stimulating discussions, as well as Professor Albert Philipse for making available the data of Ref. [15].

[1] B. Alberts, D. Bray, J. Lewis, M. Raff, K. Roberts, and J. Watson, *Molecular Biology of the Cell* (Garland, New York, 1994).
[2] L. Schadler, S. Giannaris, and P. Ajayan, Appl. Phys. Lett. **73**, 3842 (1998).
[3] K. Niskanen, *Paper Physics* (Fapet Oy, Helsinki, 1998).
[4] M. McGlockton, B. Cox, and R. McMeeking, J. Mech. Phys. Solids **51**, 1573 (2003).
[5] J. Wilhelm and E. Frey, Phys. Rev. Lett. **77**, 2581 (1996).
[6] K. Kroy and E. Frey, Phys. Rev. Lett. **77**, 306 (1996).
[7] P. A. Janmey *et al.*, J. Biol. Chem. **269**, 32 503 (1994).
[8] F. C. MacKintosh, J. Kas, and P. A. Janmey, Phys. Rev. Lett. **75**, 4425 (1995).
[9] B. Hinner, M. Tempel, E. Sackmann, K. Kroy, and E. Frey, Phys. Rev. Lett. **81**, 2614 (1998).
[10] M. L. Gardel, M. T. Valentine, J. C. Crocker, A. R. Bausch, and D. A. Weitz, Phys. Rev. Lett. **91**, 158302 (2003).
[11] M. L. Gardel, J. H. Shin, F. C. MacKintosh, L. Mahadevan, P. A. Matsudaira, and D. A. Weitz, Phys. Rev. Lett. **93**, 188102 (2004).
[12] J. Schofield, J. Text. Inst. **29**, T239 (1938).
[13] C. van Wyk, J. Text. Inst. **37**, T285 (1946).
[14] S. Toll, Polym. Eng. Sci. **38**, 1337 (1998).
[15] S. R. Williams and A. P. Philipse, Phys. Rev. E **67**, 051301 (2003).
[16] A. P. Philipse, Langmuir **12**, 1127 (1996).
[17] J. Wilhelm and E. Frey, Phys. Rev. Lett. **91**, 108103 (2003).
[18] D. A. Head, A. J. Levine, and F. C. MacKintosh, Phys. Rev. Lett. **91**, 108102 (2003).
[19] D. A. Head, A. J. Levine, and F. C. MacKintosh, Phys. Rev. E **68**, 061907 (2003).
[20] M. Allen and D. Tildesley, *Computer Simulations of Liquids* (Clarendon Press, Oxford, 1987).
[21] S. Timoshenko and J. Goodier, *Theory of Elasticity* (McGraw-Hill, New York, 1969).
[22] K. Johnson, *Contact Mechanics* (Cambridge University Press, Cambridge, 1985).
[23] Z. Neda, R. Florian, and Y. Bréchet, Phys. Rev. E **59**, 3717 (1999).
[24] R. Christensen, Int. J. Solids Struct. **37**, 93 (2000).
[25] L. Gibson and M. Ashby, *Cellular Solids: Structure and Properties* (Pergamon, Oxford, 1988).